

Shear Waves Dispersion in Cylindrically Structured Cancellous Viscoelastic Bones

I.V. Andrianov, V.V. Danishevs'kyi, and J. Awrejcewicz

Abstract In this chapter we study anti-plane shear waves propagating through a cylindrically structured cancellous bone represented by a two-dimensional mesh of elastic trabeculae filled by a viscous marrow. In the long-wave limit, the original heterogeneous medium can be approximately substituted by a homogeneous one characterized by an effective complex shear modulus. The effect of dispersion is caused by the transmission of mechanical energy to heat due to the viscosity of the marrow (viscoelastic damping). We derive an approximate analytical solution using the asymptotic homogenization method; the cell problem is solved by means of a boundary shape perturbation and a lubrication theory approaches. For short waves, when the wavelength is comparable to the trabeculae size, the effect of dispersion is caused by successive reflections and refractions of local waves at the trabecula-marrow interfaces (Bloch dispersion). Decrease in the wavelength reveals a sequence of pass and stop frequency bands, so the heterogeneous bone can act like a discrete wave filter.

I.V. Andrianov (✉)

Department of General Mechanics, RWTH Aachen University, Templergraben 64,
52056 Aachen, Germany

e-mail: andrianov@gmail.com

V.V. Danishevs'kyi

Department of Structural Mechanics and Strength of Materials, Prydniprov's'ka State Academy of
Civil Engineering and Architecture, Chernyshevs'kogo 24a, Dnipropetrovs'k 49600, Ukraine

e-mail: vdanish@ukr.net

J. Awrejcewicz

Department of Automation, Lodz University of Technology, Biomechanics and Mechatronics,
1/15 Stefanowski St., 90-924 Lodz, Poland

Department of Vehicles, Warsaw University of Technology, 84 Narbutta Str.,
02-524 Warsaw, Poland

e-mail: jan.awrejcewicz@p.lodz.pl

1 Introduction

Animal and human bones are heterogeneous materials with a complicated hierarchical structure. Bone tissues occur in the two main forms: as a dense solid (cortical or compact bone) and as a porous medium filled by a viscous marrow (trabecular or cancellous bone) [17]. The basic mechanical discrepancy between these two types consists in their relative densities measured by a volume fraction of solids. Both types can be found in the most bones of the body. A classical example of the macroscopic bone structure can be given by the long bones (e.g., humerus, femur, and tibia). They include an outer shell of a dense cortical tissue surrounding an inner core of a porous cancellous tissue.

The microstructure of cancellous bones is often described by two- or three-dimensional mesh of interconnected rods and plates [12, 17, 21]. Despite the obvious simplicity, such idealized models can provide a satisfactory agreement between theoretical predictions and experimental results for the mechanical properties of real bones [10, 11, 15, 19, 25]. In the present paper, we shall deal with a two-dimensional model of cylindrically structured cancellous bones.

Williams and Lewis [27] considered a real 2D section of a trabecular bone and evaluated its elastic constants using the plane-strain finite elements method. The developed approach enables one to predict mechanical properties of cylindrically structured cancellous bones basing on the morphological measurements in the transverse plane.

A challenging problem consists in the detection of the bone structure using non-invasive measurements. The inverse homogenization approach (“dehomogenization procedure”) [7] can help to derive information about the microgeometry of the bone tissue from the magnitudes of static effective moduli. However, the static moduli supply only limited morphological data. Much more information can be obtained studying dynamic response of the bones. Measuring velocities and attenuation of acoustic waves at different frequencies provide us with additional information about the microstructure. Generally, frequency-dependent dynamic properties of the bone may be considered as a kind of “identification portrait”, which is unique for every sample. The larger is the explored frequency range, the more accurate is the “portrait” that can be compiled. This should give a possibility to detect even very small variations of the internal bone texture.

Acoustic waves propagating through cancellous bones undergo dispersion and damping. There are two different physical effects influencing on the dynamic properties of the bone: (i) transmission of mechanical energy to heat due to the viscosity of the marrow (viscoelastic damping and dispersion) [16] and (ii) successive reflections and refractions of local waves at the trabecula-marrow interfaces (Bloch dispersion) [2, 20]. From the theoretical standpoint, both effects are realized simultaneously. However, their intensities are very frequency dependent. For many real materials the effects of viscoelastic damping and Bloch dispersion are observed in rather distant frequency ranges. In such a case they can be analyzed separately.

We study propagation of anti-plane shear waves through a 2D cylindrically structured cancellous bones. In our work, we have shown what kind of dispersion mechanism is dominant in the propagation of viscoelastic waves in the bone. This is an important theoretical result, because it allows choosing an adequate simulation

model for the solution of this class of problems. Namely, it is necessary to consider Bloch dispersion and at the same time viscoelastic effects can be neglected, i.e. use an elastic model of the media.

The input dynamic problem is formulated in Sect. 2. In Sect. 3, the long-wave limit is considered. The solution is evaluated by means of the asymptotic homogenization procedure, and the effect of viscoelastic damping is predicted. In Sect. 4, the short-wave case is studied and the effect of Bloch dispersion is analyzed by means of the plane-wave expansion method. Conclusive remarks are presented in Sect. 5.

2 Input Dynamic Problem

We study transverse anti-plane shear waves propagating in the x_1x_2 plane through a regular cancellous structure consisting of a spatially infinite elastic matrix (trabeculae) $\Omega^{(1)}$ and viscous inclusions (marrow) $\Omega^{(2)}$ (Fig. 1). The governing two-dimensional wave equation is

$$\nabla_x (G \nabla_x u) = \rho \frac{\partial^2 u}{\partial t^2}, \tag{1}$$

where G is the complex shear modulus, ρ is the mass density, u is the longitudinal displacement (in the x_3 direction), and $\nabla_x = \mathbf{e}_1 \partial/\partial x_1 + \mathbf{e}_2 \partial/\partial x_2$, $\mathbf{e}_1, \mathbf{e}_2$ are the unit Cartesian vectors.

Due to the heterogeneity of the medium, the physical properties G and ρ are represented by piecewise continuous functions of co-ordinates:

$$G(\mathbf{x}) = G^{(a)}, \quad \rho(\mathbf{x}) = \rho^{(a)}, \text{ for } \mathbf{x} \in \Omega^{(a)}, \quad \mathbf{x} = x_1 \mathbf{e}_1 + x_2 \mathbf{e}_2. \tag{2}$$

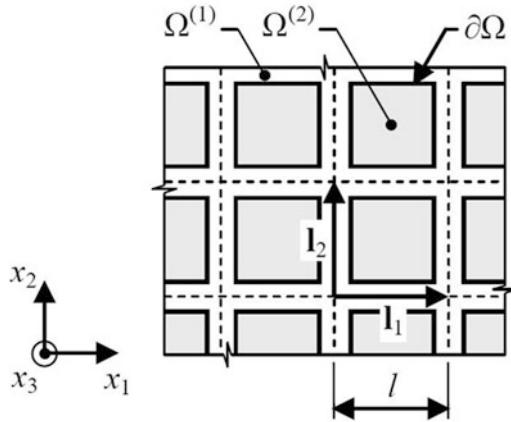


Fig. 1 Cancellous structure under consideration

Here and in the sequel the superscript (a) denotes different components of the structure $a = 1, 2$. In Eq. (2), $G^{(1)}$ is the real shear modulus of the elastic matrix and $G^{(2)}$ is the frequency-dependent imaginary shear modulus of the marrow. Following the linear theory of viscoelasticity, we can set $G^{(2)} = i\omega\eta^{(2)}$, where ω is the frequency of a harmonic wave and $\eta^{(2)}$ is the viscosity of the marrow.

Equation (1) can be written in the equivalent form:

$$G^{(a)} \nabla_{xx}^2 u^{(a)} = \rho^{(a)} \frac{\partial^2 u^{(a)}}{\partial t^2}, \quad (3)$$

$$\{u^{(1)} = u^{(2)}\} \Big|_{\partial\Omega}, \quad \left\{ G^{(1)} \frac{\partial u^{(1)}}{\partial \mathbf{n}} = G^{(2)} \frac{\partial u^{(2)}}{\partial \mathbf{n}} \right\} \Big|_{\partial\Omega}, \quad (4)$$

where $\nabla_{xx}^2 = \partial^2/\partial x_1^2 + \partial/\partial x_2^2$, $\partial/\partial \mathbf{n}$ is the normal derivative to the contour $\partial\Omega$. From the physical standpoint, Eqs. (4) means the perfect bonding conditions at the trabecula-marrow interface $\partial\Omega$.

3 Long-Wave Approach: Asymptotic Homogenization

3.1 Two-Scale Asymptotic Procedure

We start with the case when the wavelength L is essentially larger than the internal size l of the cancellous structure $l \ll L$. The original heterogeneous bone can be approximately substituted by a homogeneous one with a certain homogenized (*effective*) complex shear modulus G_0 . Such an approach neglects local reflections and refractions of the waves on microlevel. The effect of dispersion is caused by the transmission of the mechanical energy of the acoustic wave to heat due to the viscosity of the marrow.

Let us study the input boundary value problem (3), (4) by the asymptotic homogenization method [4]. In order to separate macro- and microscale components of the solution we introduce so-called *slow* \mathbf{x} and *fast* \mathbf{y} co-ordinate variables

$$\mathbf{x} = \mathbf{x}, \quad \mathbf{y} = \varepsilon^{-1} \mathbf{x}, \quad (5)$$

where $\mathbf{y} = y_1 \mathbf{e}_1 + y_2 \mathbf{e}_2$, $\varepsilon = l/L$ is a natural small parameter, and search the displacement as an asymptotic expansion

$$u^{(a)} = u_0(\mathbf{x}) + \varepsilon u_1^{(a)}(\mathbf{x}, \mathbf{y}) + \varepsilon^2 u_2^{(a)}(\mathbf{x}, \mathbf{y}) + \dots \quad (6)$$

The first term u_0 of expansion (6) represents the homogenized part of the solution; it changes slowly within the whole sample of the bone and does not depend on the fast co-ordinates ($\partial u_0/\partial y_1 = \partial u_0/\partial y_2 = 0$). The next terms, $u_i^{(a)}$, $i = 1, 2, 3, \dots$, provide corrections of the orders ε^i and describe local variations of the displacements on microlevel.

The differential operators read

$$\nabla_x = \nabla_x + \varepsilon^{-1} \nabla_y, \quad \nabla_{xx}^2 = \nabla_{xx}^2 + 2\varepsilon^{-1} \nabla_{xy}^2 + \varepsilon^{-2} \nabla_{yy}^2, \quad (7)$$

where $\nabla_y = \mathbf{e}_1 \partial / \partial y_1 + \mathbf{e}_2 \partial / \partial y_2$, $\nabla_{xy}^2 = \partial^2 / (\partial x_1 \partial y_1) + \partial^2 / (\partial x_2 \partial y_2)$, $\nabla_{yy}^2 = \partial^2 / \partial y_1^2 + \partial^2 / \partial y_2^2$.

Splitting the input problems (3), (4) with respect to ε leads to a recurrent sequence of cell boundary value problems:

$$G^{(a)} \left(\nabla_{xx}^2 u_{i-2}^{(a)} + 2\nabla_{xy}^2 u_{i-1}^{(a)} + \nabla_{yy}^2 u_i^{(a)} \right) = \rho^{(a)} \frac{\partial^2 u_{i-2}^{(a)}}{\partial t^2}, \quad (8)$$

$$\left\{ u_i^{(1)} = u_i^{(2)} \right\} \Big|_{\partial\Omega},$$

$$\left\{ G^{(1)} \left(\frac{\partial u_{i-1}^{(1)}}{\partial \mathbf{n}} + \frac{\partial u_i^{(1)}}{\partial \mathbf{m}} \right) = G^{(2)} \left(\frac{\partial u_{i-1}^{(2)}}{\partial \mathbf{n}} + \frac{\partial u_i^{(2)}}{\partial \mathbf{m}} \right) \right\} \Big|_{\partial\Omega}, \quad (9)$$

where $i = 1, 2, 3, \dots$, $u_{-1}^{(a)} = 0$, $\partial / \partial \mathbf{m}$ is the normal derivative to the interface $\partial\Omega$ written in fast variables.

For a spatially periodic medium, the terms $u_i^{(a)}$ have to satisfy the conditions of periodicity

$$u_i^{(a)}(\mathbf{x}, \mathbf{y}) = u_i^{(a)}(\mathbf{x}, \mathbf{y} + \mathbf{L}_p), \quad (10)$$

and normalization

$$\langle u_i^{(a)} \rangle = 0, \quad (11)$$

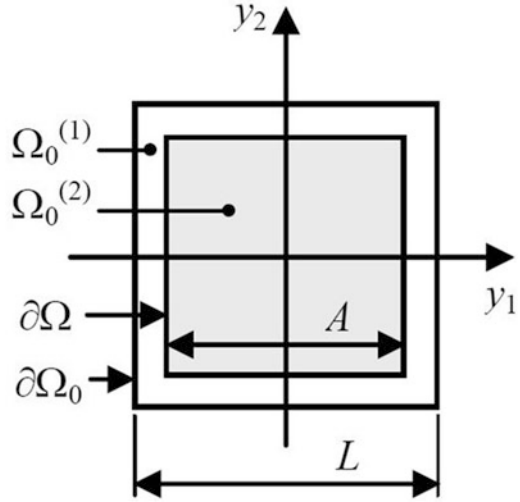
where $\mathbf{L}_p = \varepsilon^{-1} \mathbf{l}_p$, $\mathbf{l}_p = p_1 \mathbf{l}_1 + p_2 \mathbf{l}_2$, $p_1, p_2 = 0, \pm 1, \pm 2, \dots$, $\mathbf{l}_1, \mathbf{l}_2$ are the fundamental translation vectors of the cancellous structure (see Fig. 1),

$$\langle \cdot \rangle = \frac{1}{S_0} \left(\iint_{\Omega_0^{(1)}} (\cdot) dy_1 dy_2 + \iint_{\Omega_0^{(2)}} (\cdot) dy_1 dy_2 \right) \quad (12)$$

is the homogenizing operator over the unit cell domain $\Omega_0 = \Omega_0^{(1)} + \Omega_0^{(2)}$ (Fig. 2), and $S_0 = L^2$ is the area of the unit cell in the fast co-ordinates.

Conditions (10) and (11) can be approximately replaced by zero boundary conditions for some functions in the center and along the outer contour $\partial\Omega_0$ of the unit cell:

Fig. 2 Periodically repeated unit cell



$$\left\{ u_i^{(2)} = 0 \right\} \Big|_{x,y=0}, \quad \left\{ u_i^{(1)} = 0 \right\} \Big|_{\partial\Omega_0}. \tag{13}$$

For 1D problems, Eq. (13) appears entirely equivalent to Eqs. (10) and (11). For 2D problems, replacing the periodicity conditions by zero boundary conditions increases stiffness of the system and, thus, provides an upper bound for the effective properties. Analysis of numerical examples has shown that discrepancy between the final solutions in both cases is not essential [1, 3], whereas utilizing approximation (13) leads to a sufficient simplification of the cell problems.

Due to the periodicity of $u_i^{(a)}$ (10), Eqs. (8) and (9) can be considered within only one distinguished unit cell. Solution of the cell problems (8), (9), (13) at $i = 1$ determines the term $u_1^{(a)}$. In order to find the effective modulus G_0 , the homogenizing operator (12) is applied to Eq. (8) at $i = 2$. The terms $u_2^{(a)}$ are eliminated by means of Green's theorem, which together with the boundary conditions (9) and the periodicity relation (10) implies

$$\left\langle G^{(a)} \left(\nabla_{xy}^2 u_i^{(a)} + \nabla_{yy}^2 u_{i+1}^{(a)} \right) \right\rangle = 0.$$

As a result, the homogenized wave equation of the order ε^0 is obtained:

$$\left\langle G^{(a)} \left(\nabla_{xx}^2 u_0 + \nabla_{xy}^2 u_1^{(a)} \right) \right\rangle = \langle \rho^{(a)} \rangle \frac{\partial^2 u_0}{\partial t^2}. \tag{14}$$

Substituting here expressions for $u_1^{(a)}$ evaluated below we shall come to a macroscopic wave equation

$$G_0 \nabla_{xx}^2 u_0 = \rho_0 \frac{\partial^2 u_0}{\partial t^2}, \tag{15}$$

where $\rho_0 = (1 - c^{(2)})\rho^{(1)} + c^{(2)}\rho^{(2)}$ is the effective mass density, $c^{(2)}$ is the volume fraction of the inclusions, $c^{(2)} = A/S_0$, A is the size of the inclusion (Fig. 2). The effective modulus G_0 can be derived after evaluation of the integrals in Eq. (14).

Below we find approximate solutions of the cell problem (8), (9), (13) and determine the effective shear modulus G_0 using a boundary shape perturbation and lubrication theory approaches.

3.2 The Case $c^{(2)} \ll 1$: Boundary Shape Perturbation

If the volume fraction $c^{(2)}$ of the marrow inclusions is relatively small, the square shapes of the domains $\Omega^{(1)}$, $\Omega^{(2)}$ can be approximately substituted by the equal circles of radii R_1 , R_2 so that $c^{(2)} = R_2^2/R_1^2$ (Fig. 3). This simplification can be considered as the first approximation of the method of the boundary shape perturbation [1, 14].

Let us introduce in the unit cell the polar co-ordinates $r^2 = y_1^2 + y_2^2$, $\tan \theta = y_2/y_1$. Equations (8), (9), and (13) at $i = 1$ read

$$\frac{\partial^2 u_1^{(a)}}{\partial r^2} + \frac{1}{r} \frac{\partial u_1^{(a)}}{\partial r} + \frac{1}{r^2} \frac{\partial^2 u_1^{(a)}}{\partial \theta^2} = 0, \tag{16}$$

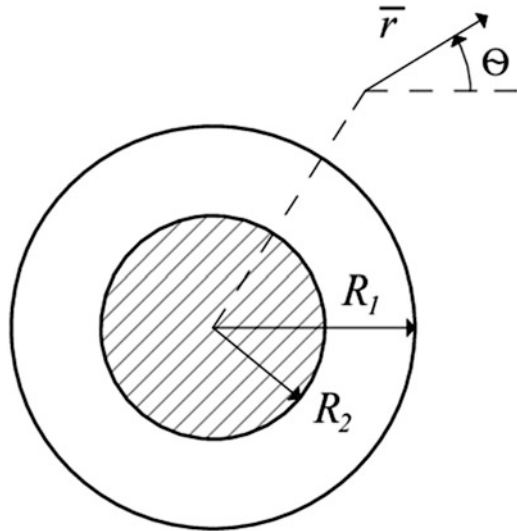


Fig. 3 Simplification of the unit cell in the case $c^{(2)} \ll 1$

$$\left. \begin{aligned} \left\{ u_1^{(1)} = u_1^{(2)} \right\} \Big|_{r=R_2}, \\ \left\{ G^{(1)} \left(\frac{\partial u_0}{\partial \mathbf{n}} + \frac{\partial u_1^{(1)}}{\partial r} \right) = G^{(2)} \left(\frac{\partial u_0}{\partial \mathbf{n}} + \frac{\partial u_1^{(2)}}{\partial r} \right) \right\} \Big|_{r=R_2}, \end{aligned} \right. \quad (17)$$

$$\left. \begin{aligned} \left\{ u_1^{(2)} = 0 \right\} \Big|_{r=0}, \quad \left\{ u_1^{(1)} = 0 \right\} \Big|_{r=R_1}, \end{aligned} \right. \quad (18)$$

where $\partial/\partial \mathbf{n} = \cos \theta \partial/\partial x_1 + \sin \theta \partial/\partial x_2$.

Solution of the simplified cell problem (16)–(18) is

$$u_1^{(a)} = \left(C_1^{(a)} r + C_2^{(a)} r^{-1} \right) \frac{\partial u_0}{\partial \mathbf{n}}, \quad (19)$$

$$C_1^{(1)} = \frac{(\lambda^{(2)} - 1) c^{(2)}}{\lambda^{(2)} + 1 - c^{(2)} (\lambda^{(2)} - 1)}, \quad C_2^{(1)} = -\frac{(\lambda^{(2)} - 1) R_2^2}{\lambda^{(2)} + 1 - c^{(2)} (\lambda^{(2)} - 1)},$$

$$C_1^{(2)} = -\frac{(\lambda^{(2)} - 1) (1 - c^{(2)})}{\lambda^{(2)} + 1 - c^{(2)} (\lambda^{(2)} - 1)}, \quad C_2^{(2)} = 0,$$

where $\lambda^{(2)} = G^{(2)}/G^{(1)}$.

Substituting expressions (19) into the homogenized equation (14), we obtain the effective modulus G_0 in the closed analytical form:

$$\lambda_0 = \frac{\lambda^{(2)} + 1 + c^{(2)} (\lambda^{(2)} - 1)}{\lambda^{(2)} + 1 - c^{(2)} (\lambda^{(2)} - 1)}, \quad (20)$$

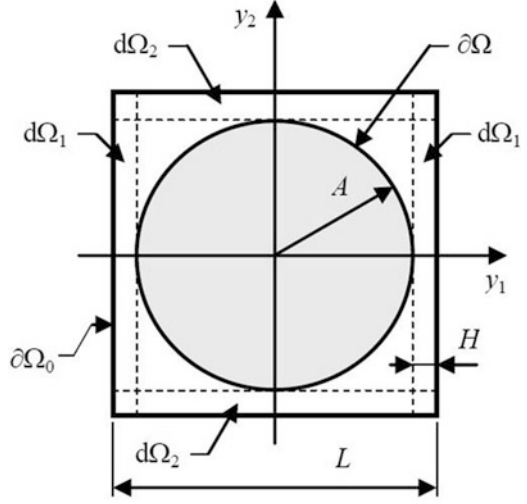
where $\lambda_0 = G_0/G^{(1)}$.

It should be noted that solution (20) is precisely the same as can be obtained by the composite cylinder assemblage model and by the generalized self-consistent scheme [8].

3.3 The Case $c^{(2)} \rightarrow 1$: Lubrication Theory

In the case of densely packed marrow inclusions, when the volume fraction $c^{(2)}$ is close to unit, $c^{(2)} \rightarrow 1$, an asymptotic solution of the cell problem can be obtained using as a natural small parameter the non-dimensional width $\delta = H/L$ of the trabecula (Fig. 4). Let us suppose $\delta < 1$. Being restricted by the $O(\delta^0)$ approximation,

Fig. 4 Unit cell in the case $c^{(2)} \rightarrow 1$



for the matrix strips $d\Omega_1$, $d\Omega_2$, which separate neighbouring inclusions, one can show

$$\frac{\partial^2 u_1^{(1)}}{\partial y_1^2} \gg \frac{\partial^2 u_1^{(1)}}{\partial y_2^2} \quad \text{for } \mathbf{y} \in d\Omega_1, \quad \frac{\partial^2 u_1^{(1)}}{\partial y_1^2} \ll \frac{\partial^2 u_1^{(1)}}{\partial y_2^2} \quad \text{for } \mathbf{y} \in d\Omega_2. \quad (21)$$

The physical meaning of estimations (21) is that in the narrow strip $d\Omega_1$ the variation of local stresses in the direction y_1 is dominant and, hence, the term $\partial^2 u_1^{(1)}/\partial y_2^2$ can be neglected in comparison with $\partial^2 u_1^{(1)}/\partial y_1^2$. Vice versa, in the strip $d\Omega_2$, the dominant variation of the local stress field takes place in the direction y_2 , so the term $\partial^2 u_1^{(1)}/\partial y_1^2$ can be neglected in comparison with $\partial^2 u_1^{(1)}/\partial y_2^2$. Such a simplification is similar to the basic idea of the well-known lubrication theory, which was used in the theory of composites for many years [8, 9].

Following estimations (21), in the $O(\delta^0)$ approximation, Eq. (8) reads

$$G^{(1)} \left(\frac{\partial^2 u_{i-2}^{(1)}}{\partial x_s^2} + 2 \frac{\partial^2 u_{i-1}^{(1)}}{\partial x_s \partial y_s} + \frac{\partial^2 u_i^{(1)}}{\partial y_s^2} \right) = \rho^{(1)} \frac{\partial^2 u_{i-2}^{(1)}}{\partial t^2}, \quad (22)$$

$$G^{(2)} \left(\nabla_{xx}^2 u_{i-2}^{(2)} + 2 \nabla_{xy}^2 u_{i-1}^{(2)} + \nabla_{yy}^2 u_i^{(2)} \right) = \rho^{(2)} \frac{\partial^2 u_{i-2}^{(2)}}{\partial t^2}$$

Solution of the simplified cell problems (9), (13), (22) at $i = 1$ is

$$u_1^{(2)} = - \frac{(1 - \sqrt{c^{(2)}})(\lambda^{(2)} - 1)}{\lambda^{(2)} - \sqrt{c^{(2)}}(\lambda^{(2)} - 1)} y_s \frac{\partial u_0}{\partial x_s}, \quad (23)$$

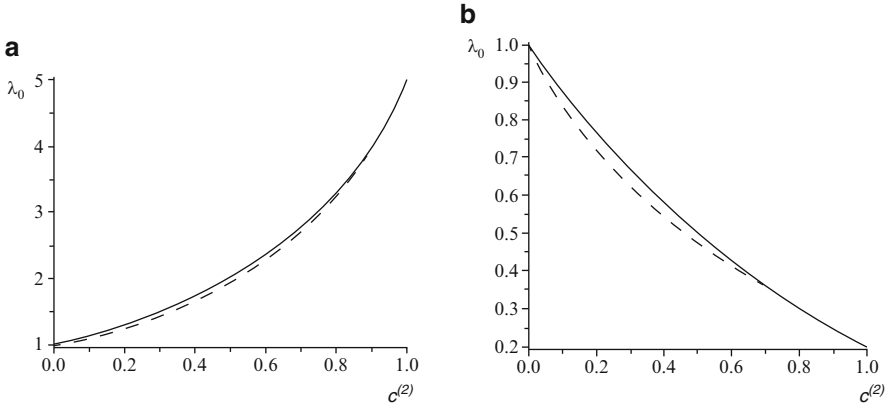


Fig. 5 Effective modulus in the elastic case. *Solids*—formula (20), *dashes*—formula (24). (a) $\lambda^{(2)} = 5$. (b) $\lambda^{(2)} = 0.2$

$$u_1^{(1)} = -\frac{\sqrt{c^{(2)}} (\lambda^{(2)} - 1)}{\lambda^{(2)} - \sqrt{c^{(2)}} (\lambda^{(2)} - 1)} \left(\frac{L}{2} - y_s \right) \frac{\partial u_0}{\partial x_s} \quad \text{at } y_s > 0,$$

$$u_1^{(1)} = \frac{\sqrt{c^{(2)}} (\lambda^{(2)} - 1)}{\lambda^{(2)} - \sqrt{c^{(2)}} (\lambda^{(2)} - 1)} \left(\frac{L}{2} + y_s \right) \frac{\partial u_0}{\partial x_s} \quad \text{at } y_s < 0,$$

where $s = 1, 2$.

For the effective shear modulus we obtain

$$\lambda_0 = \frac{\lambda^{(2)} - \sqrt{c^{(2)}} (1 - \sqrt{c^{(2)}}) (\lambda^{(2)} - 1)}{\lambda^{(2)} - \sqrt{c^{(2)}} (\lambda^{(2)} - 1)}. \quad (24)$$

Numerical results, calculated by formulas (20) and (24), are very close (except the case $\lambda^{(2)} < 1$, $c^{(2)} \rightarrow 0$). This is illustrated at Fig. 5 for real values of $\lambda^{(2)}$, which correspond to elastic materials. Moreover, in the limit $c^{(2)} \rightarrow 1$, the approximate solutions (20) and (24) exhibit the same asymptotic behaviour and give identical expansions for λ_0 until the order $O[(1 - c^{(2)})^2]$:

$$\lambda_0 = \lambda^{(2)} - \frac{1}{2} (\lambda^{(2)} - 1) (\lambda^{(2)} + 1) (1 - c^{(2)}) + O[(1 - c^{(2)})^2] \quad \text{at } c^{(2)} \rightarrow 1.$$

This fact reveals that for the cancellous structure under consideration, expression (20), originally obtained for the case $c^{(2)} \ll 1$, provides a reasonable approximation in the whole region of the inclusions volume fraction $0 \leq c^{(2)} \leq 1$.

3.4 Propagation of Long Waves

Let us consider a harmonic wave

$$u_0 = U \exp(-i\boldsymbol{\mu} \cdot \mathbf{x}) \exp(i\omega t), \quad (25)$$

where U is the amplitude, ω is the frequency, and $\boldsymbol{\mu} = \mu_1 \mathbf{e}_1 + \mu_2 \mathbf{e}_2$ is the wave vector and the direction of propagation is determined by the angle α , $\tan \alpha = \mu_2/\mu_1$.

Separating real $\boldsymbol{\mu}_R$ and imaginary $\boldsymbol{\mu}_I$ parts of the wave vector $\boldsymbol{\mu} = \boldsymbol{\mu}_R - i\boldsymbol{\mu}_I$, expression (25) reads

$$u_0 = U \exp(-\boldsymbol{\mu}_I \cdot \mathbf{x}) \exp(-i\boldsymbol{\mu}_R \cdot \mathbf{x}) \exp(i\omega t). \quad (26)$$

Here $\mu_I = |\boldsymbol{\mu}_I|$ is the attenuation factor and $\mu_R = |\boldsymbol{\mu}_R| = 2\pi/L$ is the wave number.

For the viscoelastic composite medium, the effective complex modulus G_0 , the attenuation coefficient μ_I and the phase velocity $v_p = \omega/\mu_R$ depend on the frequency of the travelling signal. Substituting expression (26) into the macroscopic wave equation (15), we obtain

$$(G_{0,R} + iG_{0,I})(\mu_I + i\mu_R)^2 = -\rho_0\omega^2, \quad (27)$$

where $G_{0,R}$, $G_{0,I}$ are, respectively, the real and the imaginary part of G_0 , $G_0 = G_{0,R} + iG_{0,I}$. Collecting in Eq. (27) the terms at 1 and i , after routine transformations we derive

$$\mu_I = \mu_R \tan(\varphi_0/2), \quad v_p^2 = \frac{v_0^2}{\cos(\varphi_0/2)^2}, \quad (28)$$

where $\tan(\varphi_0) = G_{0,I}/G_{0,R}$ is the effective loss tangent and $v_0 = \sqrt{|G_0|/\rho_0}$ is the effective velocity in the elastic case.

Adopting for G_0 the solution (20), we obtain

$$G_0 = G^{(1)} \frac{G^{(1)}(1-c^{(2)}) + i\omega\eta^{(2)}(1+c^{(2)})}{G^{(1)}(1+c^{(2)}) + i\omega\eta^{(2)}(1-c^{(2)})}, \quad (29)$$

$$\tan(\varphi_0) = \frac{4G^{(1)}c^{(2)}\omega\eta^{(2)}}{[1-(c^{(2)})^2][(G^{(1)})^2 + (\omega\eta^{(2)})^2]}.$$

In the numerical examples presented below we accept some rough estimations of the properties of the components following Bryant et al. [6], Guo [13], and Van Rietbergen and Huiskes [26]. The shear modulus of the trabeculae is $G^{(1)} = 3.85 \cdot 10^9$ Pa and the viscosity of the marrow is $\eta^{(2)} = 0.15$ Pa·s (at the room temperature of 20 °C) and $\eta^{(2)} = 0.05$ Pa·s (at the body temperature of 37 °C). The trabeculae volume fraction $c^{(1)} = 1 - c^{(2)}$ can vary from 0.05–0.1 for aged osteoporotic bones to 0.3–0.35 for young normal bones.

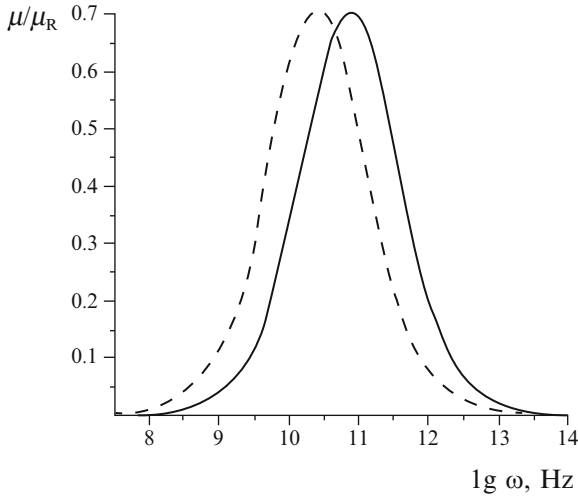


Fig. 6 Attenuation factor of a normal bone. *Solids*— $\eta^{(2)} = 0.05 \text{ Pa} \cdot \text{s}$, *dashes*— $\eta^{(2)} = 0.15 \text{ Pa} \cdot \text{s}$

Dependencies of the attenuation factor μ_I upon the frequency ω are displayed at Fig. 6 (normal bone, $c^{(1)} = 0.3$) and Fig. 7 (osteoporotic bone, $c^{(1)} = 0.1$). The dispersion effect vanishes (i) at $\omega \rightarrow 0$, when the deformation rate is small and the stiffness of the marrow is negligible, and (ii) at $\omega \rightarrow \infty$, when the deformation rate is high, so the marrow acts like a perfectly stiff medium. Decrease of the trabeculae volume fraction $c^{(1)}$ leads to the intensifying of the dispersion: the damping frequency region extends and the attenuation factor μ_I grows. Decrease in temperature (i.e. increase in the marrow viscosity $\eta^{(2)}$) leads to a reduction of the damping frequency. In any case, for physically meaningful values of the bone properties, the effect of viscoelastic damping can be observed starting from the frequencies of the order 100 MHz and higher.

It should be noted that in the long-wave limit ($l \ll L$) the cancellous structure under consideration is transversely orthotropic. The obtained solution for anti-plane shear waves is isotropic in the plane x_1x_2 , so the parameters G_0 , φ_0 do not depend on the direction of the wave propagation. The effect of anisotropy is predicted in the case of short waves (see Sect. 4).

4 Floquet-Bloch Approach: Plane-Wave Expansion Method

When the wavelength L is comparable to the internal size l of the cancellous structure, the effect of dispersion is caused by successive reflections and refractions of local waves at the trabecula-marrow interfaces. Decrease in the wavelength reveals a sequence of pass and stop frequency bands (so-called phononic bands)

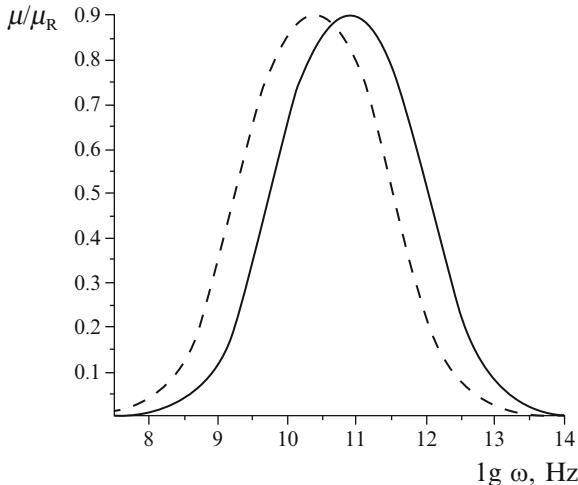


Fig. 7 Attenuation factor of an osteoporotic bone. *Solids*— $\eta^{(2)} = 0.05 \text{ Pa}\cdot\text{s}$, *dashes*— $\eta^{(2)} = 0.15 \text{ Pa}\cdot\text{s}$

[2, 20]. Thus, a heterogeneous bone can act as a discrete wave filter. If the frequency of the signal falls within a stop band, a stationary wave is excited and the neighbouring trabeculae vibrate in alternate directions. On macrolevel the amplitude of the global wave attenuates exponentially, so no propagation is possible.

In order to explore such a case, let us assume the threshold of the first stop band to be essentially lower than the viscoelastic damping frequencies. The marrow is not involved into the shear deformation, so we can set $G^{(2)} = 0$, $\rho^{(2)} = 0$.

Following the Floquet-Bloch theorem [5], a harmonic wave propagating through a periodic cancellous structure is represented in the form

$$w = F(\mathbf{x}) \exp(i\boldsymbol{\mu} \cdot \mathbf{x}) \exp(i\omega t), \tag{30}$$

where $F(\mathbf{x})$ is a spatially periodic function, $F(\mathbf{x}) = F(\mathbf{x} + \mathbf{l}_p)$.

We use the plane-wave expansion method [20, 23] and express the function $F(\mathbf{x})$ and the material properties $G(\mathbf{x})$, $\rho(\mathbf{x})$ as infinite Fourier series:

$$\begin{aligned} F(\mathbf{x}) &= \sum_{k_1=-\infty}^{\infty} \sum_{k_2=-\infty}^{\infty} A_{k_1 k_2} \exp\left[i\frac{2\pi}{l}(k_1 x_1 + k_2 x_2)\right], \\ G(\mathbf{x}) &= \sum_{k_1=-\infty}^{\infty} \sum_{k_2=-\infty}^{\infty} B_{k_1 k_2} \exp\left[i\frac{2\pi}{l}(k_1 x_1 + k_2 x_2)\right], \\ \rho(\mathbf{x}) &= \sum_{k_1=-\infty}^{\infty} \sum_{k_2=-\infty}^{\infty} C_{k_1 k_2} \exp\left[i\frac{2\pi}{l}(k_1 x_1 + k_2 x_2)\right], \end{aligned} \tag{31}$$

where

$$B_{k_1 k_2} = \frac{1}{l^2} \iint G(\mathbf{x}) \exp \left[-i \frac{2\pi}{l} (k_1 x_1 + k_2 x_2) \right] dx_1 dx_2,$$

$$C_{k_1 k_2} = \frac{1}{l^2} \iint_{\Omega_0} \rho(\mathbf{x}) \exp \left[-i \frac{2\pi}{l} (k_1 x_1 + k_2 x_2) \right] dx_1 dx_2,$$

the operator $\iint_{\Omega_0} (\cdot) dx_1 dx_2$ denotes integration over a distinguished unit cell Ω_0 .

Substituting Ansatz (30) and expansions (31) into the wave equation (1) and collecting the terms $\exp[i2\pi l^{-1}(j_1 x_1 + j_2 x_2)]$, $j_1, j_2 = 0, \pm 1, \pm 2, \dots$, we come to an infinite system of linear algebraic equations for the unknown coefficients $A_{k_1 k_2}$:

$$\sum_{k_1=-\infty}^{\infty} \sum_{k_2=-\infty}^{\infty} A_{k_1 k_2} \left\{ \begin{array}{l} B_{j_1 - k_1, \left[\left(\frac{2\pi}{l} k_1 + \mu_1 \right) \left(\frac{2\pi}{l} j_1 + \mu_1 \right) + \right.} \\ j_2 - k_2 \\ \left. + \left(\frac{2\pi}{l} k_2 + \mu_2 \right) \left(\frac{2\pi}{l} j_2 + \mu_2 \right) \right] - C_{j_1 - k_1, \omega^2} \\ j_2 - k_2 \end{array} \right\} = 0. \quad (32)$$

System (32) has a nontrivial solution if and only if the determinant of the matrix of the coefficients is zero. Equating the determinant to zero, we derive a dispersion relation for ω and μ . It should be noted that the plane-wave expansion method does not use explicitly the bonding conditions (4), whereas they are “embedded” implicitly into Eq. (1) and expansions (31).

To illustrate the appearance of phononic band gaps, let us rewrite Ansatz (30) separating real μ_R and imaginary μ_I parts of the wave vector $\boldsymbol{\mu} = \boldsymbol{\mu}_R - i\boldsymbol{\mu}_I$:

$$w = F(\mathbf{x}) \exp(-\boldsymbol{\mu}_I \cdot \mathbf{x}) \exp(i\boldsymbol{\mu}_R \cdot \mathbf{x}) \exp(i\omega t). \quad (33)$$

The imaginary part $\mu_I \equiv |\boldsymbol{\mu}_I|$ represents the attenuation factor. Frequency regions where $\mu_I \neq 0$ correspond to stop bands (signal (30) attenuates exponentially), while regions where $\mu_I = 0$ correspond to pass bands.

In numerical examples the dispersion relations are calculated approximately by the truncation of the infinite system (32) supposing $-j_{\max} \leq j_s \leq j_{\max}$. The number of the kept equations is $(2j_{\max} + 1)^2$. We expect that increase in j_{\max} shall improve the accuracy of the solution. From the physical point of view, such a truncation means cutting off the higher frequencies.

Figure 8 displays dispersion curves for a normal bone with the following properties of the trabecular tissue: $G^{(1)} = 3.85 \cdot 10^9$ Pa, $\rho^{(1)} = 1900$ kg/m³, $c^{(1)} = 0.3$. Calculations are performed at $j_{\max} = 3$. The diagram consists of two (left and

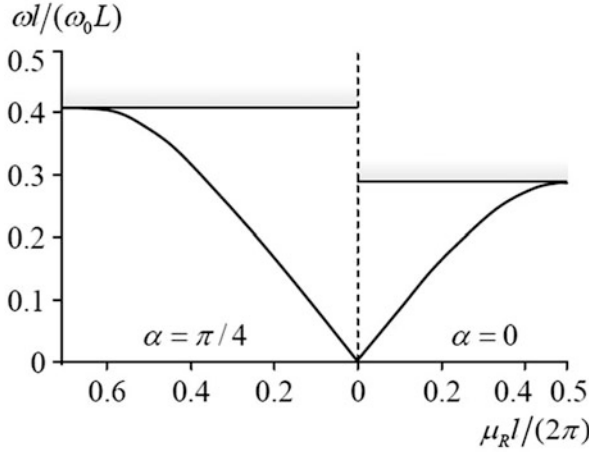


Fig. 8 Dispersion curves of a normal bone

right) parts separated by a vertical dash line. The right part displays a solution for the orthogonal direction ($\alpha = 0$) and the left part for the diagonal direction ($\alpha = \pi/4$) of the wave propagation. The results for the frequency ω are normalized to $\omega_0 = v_0 \mu_R = 2\pi v_0 / L$. We can observe that in the long-wave case ($\omega \rightarrow 0, l/L \rightarrow 0$) the solution is isotropic. However, with the increase in ω and decrease in L , the cancellous structure exhibits an anisotropic behaviour.

Shaded areas at Fig. 8 indicate the threshold of the first stop bands. Let us estimate the corresponding values ω_s of the frequency. We obtain $\omega_s l / (\omega_0 L) \approx 0.29$ at $\alpha = 0$ and $\omega_s l / (\omega_0 L) \approx 0.41$ at $\alpha = \pi/4$. The typical length of trabeculae is about $l \approx 10^{-3}$ m. Taking into account $\omega_0 = 2\pi v_0 / L$, $v_0 = \sqrt{G_0 / \rho_0}$, we derive $\omega_s \approx 2.0$ MHz at $\alpha = 0$ and $\omega_s \approx 2.8$ MHz at $\alpha = \pi/4$.

5 Conclusions

For anti-plane shear waves the effect of Bloch dispersion, caused by the heterogeneity of cancellous bones, appears at essentially lower frequencies than the effect of viscoelastic damping, caused by the viscosity of the marrow. Bloch dispersion is expected to play the primary role in the processes of ultrasonic diagnostic, which usually deals with acoustic waves in the regions 1–10 MHz. The viscoelastic damping can be neglected until the frequency of about 100 MHz. Obtained results may be used for the development of new methods of non-invasive testing and diagnostic.

In the present paper, a perfectly regular arrangement of marrow inclusions is investigated. It is clear that the microstructure of real bones is not regular. At the same time, it has been shown in a number of studies [18, 22, 24] that regular

structures exhibit the narrowest stop bands in comparing to disordered systems. Thus, the obtained solutions may be treated as theoretical bounds for the stop band thresholds that appear in randomly disordered bone tissues.

Acknowledgments This work is supported by the Alexander von Humboldt Foundation (Institutional academic co-operation programme, grant no. 3.4-Fokoop-UKR/1070297), the German Research Foundation (Deutsche Forschungsgemeinschaft, grant no. WE 736/30-1).

References

1. Andrianov, I.V., Danishevs'kyy, V.V., Guillet, A., Pareige, P.: Effective properties and micro-mechanical response of filamentary composite wires under longitudinal shear. *Eur. J. Mech. A/Solids* **24**, 195–206 (2005)
2. Andrianov, I.V., Bolshakov, V.I., Danishevs'kyy, V.V., Weichert, D.: Higher-order asymptotic homogenization and wave propagation in periodic composite materials. *Proc. Roy. Soc. A Math. Phys. Eng. Sci.* **464**, 1181–1201 (2008)
3. Andrianov, I.V., Bolshakov, V.I., Danishevs'kyy, V.V., Weichert, D.: Asymptotic study of imperfect interfaces in conduction through a granular composite material. *Proc. Roy. Soc. A Math. Phys. Eng. Sci.* **466**, 2707–2725 (2010)
4. Bakhvalov, N.S., Panasenko, G.P.: *Homogenization: Averaging Processes in Periodic Media. Mathematical Problems in Mechanics of Composite Materials.* Kluwer, Dordrecht (1989)
5. Brillouin, L.: *Wave Propagation in Periodic Structures: Electric Filters and Crystal Lattices.* Dover, New York (2003)
6. Bryant, J.D., David, T., Gaskell, P.H., King, S., Lond, G.: Rheology of bovine bone marrow. *Proc. Inst. Mech. Eng. H J. Eng. Med.* **203**(2), 71–75 (1989)
7. Cherkaev, E., Ou, M.-J.Y.: Dehomogenization: reconstruction of moments of the spectral measure of the composite. *Inverse Probl.* **24**, 065008 (2008)
8. Christensen, R.M.: *Mechanics of Composite Materials.* Dover, Mineola (2005)
9. Frankel, N.A., Acrivos, A.: On the viscosity of a concentrated suspension of solid spheres. *Chem. Eng. Sci.* **22**, 847–853 (1967)
10. Galka, A., Telega, J.J., Tokarzewski, S.: A contribution to evaluation of effective moduli of trabecular bone with rod-like microstructure. *J. Theor. Appl. Mech.* **37**, 707–727 (1999)
11. Galka, A., Telega, J.J., Tokarzewski, S.: Application of homogenization to evaluation of effective moduli of linear elastic trabecular bone with plate-like structure. *Arch. Mech.* **51**, 335–355 (1999)
12. Gibson, J.L., Ashby, M.P.: *Cellular Solids: Structure and Properties.* Pergamon, Oxford (1988)
13. Guo, X.E.: Mechanical properties of cortical bone and cancellous bone tissue. In: Cowin, S.C. (ed.) *Bone Mechanics Handbook*, pp. 10-1–10-23. CRC, Boca Raton (2001)
14. Guz, A.N., Nemish, Y.N.: Perturbation of boundary shape in continuum mechanics. *Soviet Appl. Mech.* **23**(9), 799–822 (1987)
15. Hollister, S.J., Fyhire, D.P., Jepsen, K.J., Goldstein, S.A.: Application of homogenization theory to the study of trabecular bone mechanics. *J. Biomech.* **24**, 825–839 (1991)
16. Hughes, E.R., Leighton, T.G., Petley, G.M., White, P.R., Chivers, R.C.: Estimation of critical and viscous frequencies for Biot theory in cancellous bone. *Ultrasonics* **41**, 365–368 (2003)
17. Jee, W.S.S.: Integrated bone tissue physiology: anatomy and physiology. In: Cowin, S.C. (ed.) *Bone Mechanics Handbook*, pp. 1-1–1-68. CRC, Boca Raton (2001)
18. Jensen, J.S.: Phononic band gaps and vibrations in one- and two-dimensional mass-spring structures. *J. Sound Vib.* **266**, 1053–1078 (2003)
19. Kasra, M., Grynypas, M.D.: Static and dynamic finite element analyses of an idealized structural model of vertebral trabecular bone. *J. Biomech. Eng.* **120**, 267–272 (1998)

20. Kushwaha, M.S., Halevi, P., Martinez, G., Dobrzynski, L., Djafari-Rouhani, B.: Theory of acoustic band structure of periodic elastic composites. *Phys. Rev. B* **49**, 2313–2322 (1994)
21. Odgaard, A.: Qualification of cancellous bone architecture. In: Cowin, S.C. (ed.) *Bone Mechanics Handbook*, pp. 14-1–14-19. CRC, Boca Raton (2001)
22. Schraad, M.W.: On the macroscopic properties of discrete media with nearly periodic microstructures. *Int. J. Solids Struct.* **38**, 7381–7407 (2001)
23. Sigalas, M.M., Economou, E.N.: Elastic and acoustic wave band structure. *J. Sound Vib.* **158**, 377–382 (1992)
24. Thorp, O., Ruzzene, M., Baz, A.: Attenuation and localization of wave propagation in rods with periodic shunted piezoelectric patches. *Smart Mater. Struct.* **10**, 979–989 (2001)
25. Tokarzowski, S., Telega, J.J., Galka, A.: Prediction of torsional rigidities of bone filled with marrow: the application of multipoint Padé approximants. *Acta Bioeng. Biomech.* **2**, 560–566 (2000)
26. Van Rietbergen, B., Huiskes, R.: Elastic constants of cancellous bone. In: Cowin, S.C. (ed.) *Bone Mechanics Handbook*, pp. 15-1–15-24. CRC, Boca Raton (2001)
27. Williams, J.L., Lewis, J.L.: Properties and an anisotropic model of cancellous bone from the proximal tibial epiphysis. *J. Biomech. Eng.* **104**(1), 50–56 (1982)